Check for updates

ChemCatChem

Research Article
doi.org/10.1002/cctc.202101947

Chemistry Europe
European Chemical Societies Publishing

www.chemcatchem.org

3D-Printed Acidic Monolithic Catalysts for Liquid-Phase Catalysis with Enhanced Mass Transfer Properties

Sebastian Hock,[a] Christof Rein,[a] and Marcus Rose*[a]

The thriving research and development in additive manufacturing and especially 3D printing in chemical engineering and heterogeneous catalysis enables novel and innovative approaches for the shaping of catalysts. In this work, tailor-made monoliths with complex transport pore channels are designed and printed by fused deposition modelling (FDM) from polystyrene filament. Subsequently, sulfonic acid groups are introduced by sulfonation for a catalytic functionalization of the structured monoliths' accessible inner surface. As a catalytic test reaction, the aqueous phase hydrolysis of sucrose was chosen. For this reaction the functionalized monoliths exhibited a superior catalytic performance in both batch and continuous reaction mode in comparison to a macroporous sulfonic acid-functionalized ion exchange resin as commercial benchmark catalyst. This is due to the higher accessibility of the sulfonic acid groups on the surface of the monoliths' pore channels and hence, enhanced effective reaction kinetics by decreased mass transfer limitations.

Introduction

In heterogeneous catalysis the shape of the catalyst and the morphology of a fixed-bed or a structured packing in a reactor or column play a fundamental role.[1–4] Activity, selectivity, flow-related properties such as mass transfer, fluid distribution, dispersion and pressure drop are all influenced by the catalyst geometry and its packed structure.[1–4] For the precise control of these properties various packing configurations have been studied theoretically[1,3,5] and experimentally,[6] posing explicit advantages to randomly packed beds.[7] Industrial implementation of optimally structured fixed-beds is still a challenging process.[8-10] One of the most prominent class of structured packings are monolithic catalysts.[4,11] Early designs with mostly straight channels were developed to include a broad variety of different geometries, pore systems and complex channel structures.[12–13] The monolithic structures showed in general enhanced film transport and reduced pressure drop.[14–15] Emerging fabrication methods such as 3D printing played a key role in promoting the design and research process in this field.[16–18] 3D printing monoliths allows a high flexibility in design, interlocking or hierarchical channels, tailored and enhanced transport properties like increased turbulence and improved fluid/surface contact.[7,14,19–21]

Additive manufacturing methods have already been successfully deployed in various research fields facilitating applications for microfluidic devices,[22] biomaterials,[23] electrochemical devices[24] and catalysis.[25–29] The specific printing process of fused deposition modelling (FDM) features melt extrusion and the deposition of various kinds of thermoplastic polymeric filaments. Due to the resulting versatility, high speed, and low investment cost this procedure became the most commonly used 3D printing method.[27,30] The initial utilization of FDM in reaction engineering was mainly in manufacturing tailored equipment and reactors.[31] Subsequently catalyst supports and catalytic materials were prepared via this printing method.[32–34] As an early example Sorkski et al.[35] printed an active catalyst for the photo degradation of Rhodamine 6G by incorporating TiO_2 nanoparticles into ABS filament.[35] Recently Sun et al. successfully prepared a catalytic monolith for the Fenton oxidation of aromatic molecules by printing a PLA filament with an incorporated iron catalyst.[36] Another example are the nanoporous gold monoliths manufactured by Zhu et al.[37] The precise tailoring of 3D structures and the development of novel catalysts respectively catalyst supports achieved improved mass transport and reaction rates in Li et al.[7] study for syngas methanation and all the reported examples.

A great challenge for the use of FDM in catalysis is the processing of composite filaments containing active filler materials in a printable matrix material. Printable filaments typically consist of thermoplastic polymers and mostly inorganic or hybrid solid particles as filler material as several studies showed.[38–40] Recently we have reported the incorporation of nanoporous polymer particles into monolithic composite materials.[18] A major goal for catalytic applications is to incorporate active components or to catalytically activate a printed geometry.

A common route to introduce functional acidic groups in organic materials is sulfonation. The sulfonation of aromatic hydrocarbons is well established with various methods of processing.[41–47] The insertion of sulfonic acid groups in the

[a] S. Hock, C. Rein, Prof. Dr. M. Rose
Ernst-Berl-Institut für Technische und Makromolekulare Chemie
Technical University of Darmstadt
Alarich-Weiss-Str. 8
64287 Darmstadt (Germany)
E-mail: marcus.rose@tu-darmstadt.de

Supporting information for this article is available on the WWW under https://doi.org/10.1002/cctc.202101947

© 2022 The Authors. ChemCatChem published by Wiley-VCH GmbH. This is an open access article under the terms of the Creative Commons Attribution Non-Commercial NoDerivs License, which permits use and distribution in any medium, provided the original work is properly cited, the use is non-commercial and no modifications or adaptations are made.

© 2022 The Authors. ChemCatChem published by Wiley-VCH GmbH

materials of choice enables acid reactions in protic solvents.[44] There are several possible approaches to the sulfonation of polystyrene. One is the use of concentrated sulfuric acid,[41,45] another is the use of sublimated sulfur trioxide in the gas phase, which can be generated most conveniently by sublimation of oleum.[46–47] These methods were applied in this work to functionalize the obtained monoliths. Further options include the sulfonation of polystyrene (PS) with acetyl sulfate[42] or the direct synthesis of polystyrene sulfonate.[43]

A suitable model reaction for polymer-based acidic catalysts is the hydrolysis of sucrose for the following reasons. The disaccharide sucrose consists of α-D-glucose and β-D-fructose, connected over an α,β-1,2-glycosidic bond.[48–49] This bond can be hydrolysed either by enzymes, like for example invertase, or chemocatalytically by Brønsted acids (see Figure 1).[48–49] The reaction passes through a fast formed transition state with the hydrolysis of the sucrose cation as the rate limiting step resulting in a formal second order reaction.[50–52] With surplus of water in an aqueous medium and a constant catalyst mass the reaction rate can be formulated as a first order kinetic, only dependent on the sucrose concentration.[50–52] With this simplification of the kinetic model, the reaction rate constant can be calculated with the Arrhenius equation as a function of the reaction temperature.[50–52] Additionally, the optical activity of the sugars can easily be observed in detail through the change of specific rotation, making this an ideal model reaction.[50–52] Heterogeneous catalysts such as Y zeolites,[53] heteropoly acids,[50] and metal oxide catalysts such as $V_2O_5/\gamma\text{-}Al_2O_3$[54] have been characterized with the hydrolysis of sucrose. Especially well understood catalysts for this reaction are ion exchange resins such as Amberlite Ir-120[55] or Amberlyst 15.[56–58] Amberlyst 15 (EMD Millipore Corporation)[58] will be used as a benchmark catalyst to compare the 3D printed acid functionalized monoliths presented in this work. The properties of Amberlyst 15 are listed in the supporting information.

In this work we prove the advantages of solid acid-functionalized monoliths obtained by the combination of the fast FDM process with subsequent acid functionalisation. The monoliths were printed from *high impact polystyrene* (HIPS) filament and activated by sulfonation. The obtained acidic monoliths were then catalytically tested in batch and continuous processing using the hydrolysis of sucrose as a model reaction. The catalysts performance was directly compared to Amberlyst 15 as commercial acidic ion exchange resin as the most suitable benchmark catalyst. The aim was to produce tailored monoliths with superior hydrodynamic properties and thereby improved catalytic activity in a fast and cost effective manner.

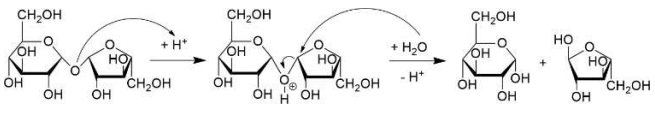

Figure 1. Acid-catalysed hydrolysis of sucrose to α-D-glucose and β-D-fructose.

Results and Discussion

3D printing of monoliths

The monoliths were prepared by FDM 3D printing based on our previous work.[18] Herein, we focused on the ABAB and ABCD structure type monoliths. The ABAB geometry consists of an AB-type packing of parallel aligned filaments with orthogonal orientation of each subsequent layer. This structure exhibits one-dimensional axial pore channels with radial connections. In the ABCD-type stacking of orthogonal alternating layers the A and C layers as well as B and D, respectively, are offset each by the diameter of one filament. Hence, there is no one-dimensional straight pore channel but rather a 3D pore system with increased tortuosity. The detailed structure (Figure 2) was designed in *Autodesk Inventor* and printed using a FDM 3D printer and high impact polystyrene (HIPS) filament. The monoliths were printed in two sizes: one for the batch reactions with a length of 4 cm, a diameter of 3 cm, and a total volume of 6.30 cm^3 for the ABAB type and 6.34 cm^3 for the ABCD type. The second type of monoliths was precisely fitted to a tubular reactor with a length of 13 cm, a diameter of 3 cm, and a volume of 27.14 cm^3 for the ABAB and 27.32 cm^3 for the ABCD type. The hydrodynamic properties pressure drop and residence time of the two monoliths were reported in our previous work[18] and are displayed in the supporting information for the different monoliths (Figure S1) with a comparsion to a CFD based simulation (Figure S2-S5) that proofs the increased mixing in the more complex channel structures compared to straight pore channels based on the cell Reynolds number and the cell velocity magnitude (Figure S2).

Sulfonation of HIPS monoliths

In order to functionalize the HIPS monoliths as acid catalysts the accessible surface was sulfonated. Different methods for the sulfonation of the accessible aryl groups were initially screened such as the sulfonation with oleum in the liquid or the gas

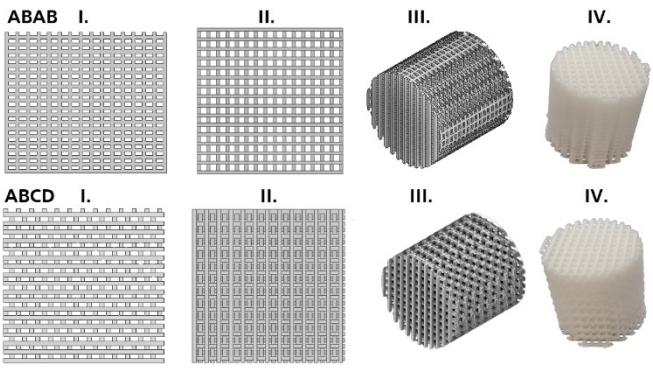

Figure 2. ABAB (top) and ABCD (bottom) grid structures in: I. front view, II. top view, III. the complete geometry of the cylinder, IV. photographs of printed HIPS-monolith.

© 2022 The Authors. ChemCatChem published by Wiley-VCH GmbH

18673899, 2022, 8, Downloaded from https://chemistry-europe.onlinelibrary.wiley.com/doi/10.1002/cctc.202101947 by Technische Universitat Darmstadt, Wiley Online Library on [18/09/2023]. See the Terms and Conditions (https://onlinelibrary.wiley.com/terms-and-conditions) on Wiley Online Library for rules of use; OA articles are governed by the applicable Creative Commons License

phase as well as using sulfuric acid at ambient temperature or 80 °C (Table 1).

The sulfonation degree was quantitatively analysed using the back titration method established in literature.[41] The standard deviation of this analytical method was determined by titrating five times a defined amount of Amberlyst 15. This resulted in a reference acid amount of 5.06 ± 0.0568 mmol g^{-1}.

Although all methods resulted in successful sulfonation especially at elevated temperatures the mechanical stability decreased significantly reduced the reproducibility. Hence, the most suitable method was the sulfonation of the HIPS monoliths with sulfuric acid at ambient temperature (22 °C) with concentrated sulfuric acid. The progressing sulfonation can be observed optically (Figure 3 I.). After one hour a homogeneous brownish coloration of the monolith was observed turning fully into black colour after six hours. Figure 3 II. shows the results of repeated experiments for the ABAB and ABCD structure for three and seven days sulfonation time. The results indicate a good reproducibility of the sulfonation degree. It has to be noted that the optical change can be a good qualitative indication to the sulfonation degree but is unfit for quantitative comparison. With longer reaction times the amount of sulfonic acid groups increased and only a minor difference in between the structures was observed.

Table 1. Display of the different tested sulfonation methods with criteria for their operational capability

Sulfonation Method	Structural integrity	Sulfonation degree [mmol g^{-1}]	Reproducibility
gas phase with oleum/SO_3	flaking of particle at water contact	up to 0,7 (after one week)	low
liquid phase with oleum	quick dissolution of monoliths	up to 0,2 (till structure loss)	low
liquid phase with hot sulfuric acid	only up to 80 °C for 120 min	up to 0,6 (till structure loss)	low
liquid phase at RT (22 °C) with sulfuric acid	ensured, only after 7 days a slight bulge is observed	up to 1,0 (after one week)	high

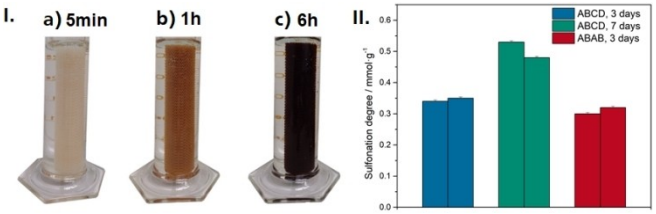

Figure 3. I. Optical change of the monoliths during sulfonation after a) five minutes, b) one hour, c) six hours; II. measured total sulfonation degree of the different monolithic structures in mmol·g^{-1}. For the estimation of reproducibility, the complete process was carried out twice. The standard deviation includes only the analytical method.

With an optimized airtight reaction vessel, the time dependency of the sulfonation was determined (Figure 4). The highest increase in the degree of sulfonation occurred over the initial 24 hours with an amount of acid sites of 0.26 mmol g^{-1}. Thereafter, the sulfonation occurred at a rather linear rate and after five days a sulfonation degree of 0.64 mmol g^{-1} was obtained. It should be noted that even after seven days there was no obvious structural change in the monoliths and sulfonation degrees above 0.7 mmol g^{-1} could be achieved. The empirical optimum in this experiment was achieved after a sulfonation time of three days with an amount of sulfonic acid groups of 0.48 mmol g^{-1} with a negligible decrease of the stability of the monoliths (Figure 4 II and III)

For comparison, the commercial reference catalyst Amberlyst 15 is a macro-porous sulfonic ion exchange acid resin with an amount of sulfonic acid groups of ca. 4.9 mmol g^{-1}.[56] This sulfonation degree is one order of magnitude higher as due to the macroporosity a significantly higher surface area is accessible compared to the monoliths with only the pore channel surface being accessible. Nevertheless, for liquid phase processes mass transfer limitation might occur for the macroporous resin and the catalyst efficiency might be significantly reduced as demonstrated in the following

Figure 4. I. Time dependency of the sulfonation of HIPS monoliths of 1–5 days; II. A batch of HIPS monoliths after three days of sulfonation; III. ABAB and ABCD monoliths before (left) and after (right) sulfonation in sulfuric acid at 22 °C for 1 d.

© 2022 The Authors. ChemCatChem published by Wiley-VCH GmbH

18673899, 2022, 8, Downloaded from https://chemistry-europe.onlinelibrary.wiley.com/doi/10.1002/cctc.202101947 by Technische Universitat Darmstadt, Wiley Online Library on [18/09/2023]. See the Terms and Conditions (https://onlinelibrary.wiley.com/terms-and-conditions) on Wiley Online Library for rules of use; OA articles are governed by the applicable Creative Commons License

Catalytic testing under batch conditions

The catalytic performance of the acidic-functionalized monoliths in comparison with Amberlyst 15 as a commercial benchmark catalyst was evaluated using the hydrolysis of sucrose as test reaction. For the experiments under batch conditions a reactor with a 3D-printed monolith holder was applied (Figure S1) to allow full immersion of the monolith in the liquid reaction mixture. It consists of a closed glass reactor with a magnetic stirring bar, an access point for temperature measurement and sampling and the above-mentioned monolith holder. The 3D-printed monolith holder enables to align the monoliths orthogonally or in parallel in regard to the direction of the liquid flow. With this setup the ABAB and the ABCD monoliths were analysed in orthogonal and parallel alignment. As a benchmark reference the commercial catalyst Amberlyst 15 was measured as suspended catalyst. All experiments were carried out at 79 °C as ideal reaction temperature based on previous work from Zajšek et al.,[51] a reaction volume of 150 mL with a sucrose concentration of 50 g L^{-1} and a stirring speed of 500 rpm. For comparable results the sulfonic acid groups of the monoliths and the benchmark catalyst were determined and the initial weight was adjusted in order to achieve a molar ratio of 0.1 for the sulfonic acid to sucrose amount for all experiments. The quantification of the reaction mixture was carried out by sampling and a calibrated offline HPLC analysis. Based on the quantitative concentration time profiles (Figure 5) the reaction rate constants (Figure 6) were calculated based on Equation 1.

$$r = -\frac{dc_s}{dt} = k \cdot c_{SH^+} \cdot c_{H_2O} \quad (1)$$

r specific reaction rate
c_s concentration of sucrose at the time t
k reaction rate constant
c_{SH^+} concentration of the sucrose cation
c_{H_2O} concentration of water

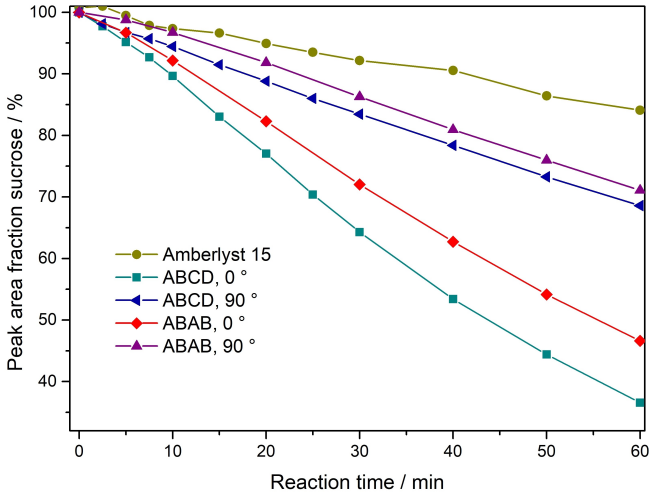

Figure 5. Time dependent conversion of sucrose in the batch reaction setup. Comparison of the monoliths in regards to the alignment and the reference catalyst Amberlyst 15 in suspension.

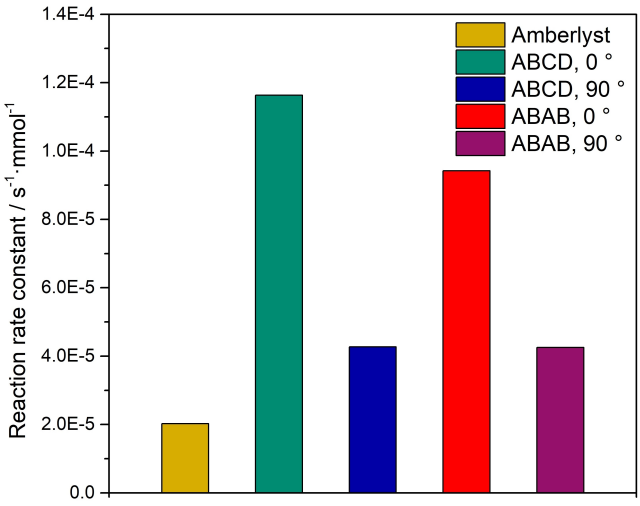

Figure 6. Reaction rate constant of the monoliths in regard to the alignment and the reference catalyst Amberlyst 15.

For both monoliths (ABAB and ABCD) the highest reaction rate constants were observed when being aligned in the direction of flow. Interestingly, the ABAB monolith with the linear pore channels exhibited a slightly lower value than the ABCD structure. In our previous research we carried out various hydrodynamic experiments and determined an up to 75% higher mean residence time of the ABCD structure in comparison to the ABAB structure for flow rates between 1–10 mL min^{-1}.[18] In the SI we also supported the experimental data with CFD simulation. The longer residence time of the ABCD structure indicates a longer contact time and a better mixing in the ABCD's pore structure with increased tortuosity and the overall better accessibility, which would validate the presented findings. Both monoliths orthogonally aligned to the direction of flow show a significantly decreased rate constant due to a decreased accessibility of the functionalized pore channels. Overall, the ABCD monolith in direction of flow exhibited a sixfold increase of the reaction rate constant in comparison to Amberlyst 15 as benchmark catalyst. This significant increase is a result of the improved accessibility of the reaction solution in the pore channel structure of the monolith that contains all catalytically active functional groups. In contrast, the macroporous ion exchange resin has much smaller pores in which mass transfer limitations occur to a much larger extend. In this case the mass transfer significantly limits the substrate conversion. This clearly demonstrates the advantage of the structuring of catalytic monoliths and well accessible surfaces. Of course, a direct comparison of the catalytic performance of suspended particles vs. a monolith in a batch reactor is only of limited significance. Therefore, experiments with a tubular reactor and a packing of the Amberlyst 15 were carried out and will be discussed in the following chapter.

© 2022 The Authors. ChemCatChem published by Wiley-VCH GmbH

18673899, 2022, 8, Downloaded from https://chemistry-europe.onlinelibrary.wiley.com/doi/10.1002/cctc.202101947 by Technische Universitat Darmstadt, Wiley Online Library on [18/09/2023]. See the Terms and Conditions (https://onlinelibrary.wiley.com/terms-and-conditions) on Wiley Online Library for rules of use; OA articles are governed by the applicable Creative Commons License

Catalytic testing with a continuously operated reactor

For the investigation of the catalytic performance under continuous process conditions a plug flow reactor setup was used as displayed in Figure S7. The monoliths were precisely modelled to fit the tube reactors dimensions. With this convenient setup an ideal, reproducible flow through the monoliths is achieved and can be directly compared to a packed bed of the commercial Amberlyst 15 spheres. Quantification of the reaction mixture was carried out as for the batch experiments by an offline HPLC. A blank experiment without any catalyst showed no detectable conversion of sucrose.

Experiments with an ABAB-monolith, an ABCD-monolith and a packed bed of Amberlyst 15 were carried out at a temperature of 80 °C and a feed with a sucrose concentration of 50.0 g L^{-1}.To determine the flow dependency each experiment was also repeated with three different volume flows (Figure 7). The tested monoliths were precisely tailored to the tubular reactor and sulfonated over the course of one day (Figure 4 III). The total amounts of sulfonic acid groups in the reactor based on the monoliths size and the resins mass in the catalyst bed were 13.24 mmol for Amberlyst 15, 3.3 mmol for the ABAB-monolith and 3.75 mmol for the ABCD-monolith. With the known number of acid groups and the measured conversion under stationary conditions the turn over frequency (TOF) could be calculated by Equation 2.

$$TOF = \frac{c_{S0} - c_s}{N_{Sulf} \cdot t} = \frac{\dot{V} \cdot c_{S0} \cdot X}{N_{Sulf}} \quad (2)$$

c_{S0} feed concentration of sucrose
c_s concentration of sucrose at the time t
N_{Sulf} number of catalytically active groups
$\dot{V}$ volume flow
X conversion

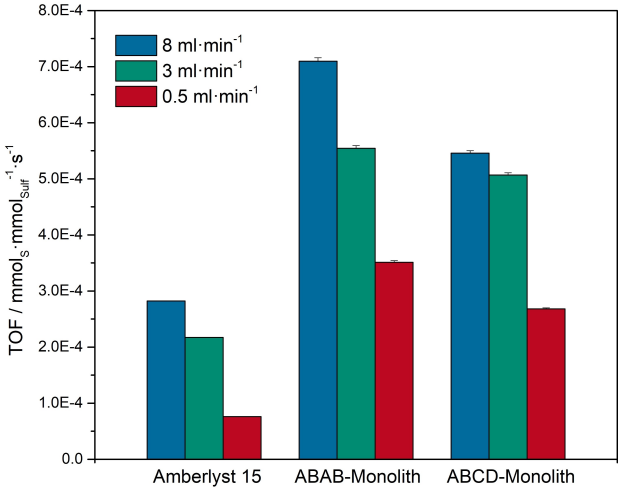

Figure 7. Comparison of the TOF of the prepared monoliths with the commercial ion exchange resin Amberlyst 15 with a continuous setup at steady state conditions.

The results displayed in Figure 7 confirm the outstanding catalytic performance of the monoliths compared to the packed bed of the ion exchange resin. The TOF of the prepared monoliths clearly exceeds the TOF of the commercial catalyst Amberlyst 15. The largest difference was measured at the lowest flow rate of 0.5 mL min^{-1}: the TOF of the ABAB-monolith was 4.6 times higher than that of the ion exchange resin while the TOF of the ABCD monolith was 3.5 times higher. With higher volume flows the difference decreases slightly. At the highest volume flow of 8 mL min^{-1} still a 2.5 times higher TOF for the ABAB and a 1.9 times higher TOF for the ABCD structure was observed.

It has to be noted that because of the significantly higher degree of functionalization a significantly smaller amount of the Amberlyst 15 was used in order to get comparable results. Due to this, the volume of the Amberlyst 15 packing is around ten times smaller than the volume of the monoliths despite exhibiting an overall higher acid amount. To ensure a proper packing of the Amberlyst 15 the reactor length was reduced by inserting a closed filling material with a channel in the size of the tubing. The repeated continuous experiments and the batch experiments shown above, however, indicate a significantly higher catalytic activity of the monoliths in comparison to the benchmark. This can be ascribed, as mentioned above, to the much better accessibility of the functional acid groups on the surface of the pore channels while the spherical resin contains most of the functional groups within its macroporous structure with severe mass transfer limitations, as schematically displayed in Figure 8. Surprisingly, the ABAB structure shows a higher TOF in comparison to the ABCD structure. In our previous research[18] we carried out various hydrodynamic experiments and determined an up to 75% higher mean residence time of the ABCD structure in comparison to the ABAB structure for flow rates between 1–10 mL min^{-1}. The longer residence time leads to a longer contact time and thus, to a smaller TOF, which is clearly verified by the experimental data. Besides the clear evidence of the superior catalytic performance of acidic monoliths compared to packed beds of spherical acidic ion exchange resins this influence of the pore channel structure on the flow properties demonstrates the

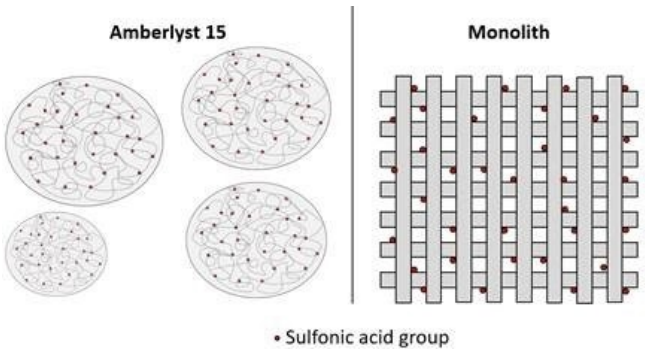

Figure 8. Schematically display of the accessibility of the sulfonic acid groups of Amberlyst 15 structure in regards to the monolithic structure.

© 2022 The Authors. ChemCatChem published by Wiley-VCH GmbH

18673899, 2022, 8, Downloaded from https://chemistry-europe.onlinelibrary.wiley.com/doi/10.1002/cctc.202101947 by Technische Universitat Darmstadt, Wiley Online Library on [18/09/2023]. See the Terms and Conditions (https://onlinelibrary.wiley.com/terms-and-conditions) on Wiley Online Library for rules of use; OA articles are governed by the applicable Creative Commons License

great potential of 3D printed structured monoliths in improving the performance of catalytic monoliths.

Conclusion

The time and cost efficient FDM-based 3D printing of common HIPS filament was successfully applied to print tailored monoliths for fixed bed reactor applications. Different methods of introducing sulfonic acid groups were tested pointing out the sulfonation at room temperature with concentrated sulfuric acid as optimal compromise. With this method a high concentration of sulfonic acid groups on the surface of the pore channels and structural integrity of the monoliths were achieved. The functionalized printed structures were compared to the commercial benchmark catalyst Amberlyst 15 in the hydrolysis of sucrose. In batch as well as in continuous process conditions the prepared monoliths showed a superior catalytic performance than the reference material due to the much better accessible functional acid groups on the surface of the pore channels and thus, avoiding severe mass transfer limitations as found for the macroporous ion exchange resin as catalyst. Also, the opportunity to tailor the pore channel structure enables a targeted optimization of the hydrodynamic properties of reactive fluids. Hence, the acquired results proof a great potential of the 3D printing in catalysis. With the presented methods, the high speed and versatility of FDM it can be directly applied to manufacture tailored catalyst with superior performance.

Experimental Section

Materials

Sulfuric acid (H_2SO_4, 96%), fuming sulfuric acid (oleum, 20 wt% SO_3), hydrochloric acid (HCl, 37%), sodium hydroxid (NaOH, 98%) and 3,3-Bis(4-hydroxyphenyl)-1(3*H*)-isobenzofuranone (Phenolphthalein) were purchased from Sigma Aldrich. D(+)-Sucrose ($C_{12}H_{22}O_1$, 99.5%), D(+)-Glucose ($C_6H_{12}O_6$, 98%) and D(−)-Fructose ($C_6H_{12}O_6$, 99.5%) were purchase from Carl Roth. HIPS filament was purchased from 3D Printshop, Berlin, and Amberlyst 15 from EMD Millipore Corporation. HCl and NaOH were diluted with deionized water to 0.01 N HCl and NaOH solution, respectively. All other chemicals were used as received.

Printing of monoliths

The monoliths were designed with the software Autodesk Inventor®. The '.stl' files were converted into '.gcode' files with the software Renkforce Repetier® host and printed with a Renkforce RF2000 3D printer using HIPS filament. The optimized printing temperature for this filament was determined with calibration towers to be 220 °C with a heat bed temperature of 90 °C for optimal adhesion.

Sulfonation of HIPS-monoliths and determination of the sulfonation degree

The respective printed HIPS monoliths were placed in 96 wt% H_2SO_4 and completely submerged. After the respective reaction times ranging from 1 hour to 7 days the reaction was stopped by removing the monoliths from the solution and subsequent washing with water until a neutral pH was achieved. The sulfonation degree was determined in accordance to the procedure described by Lei et al.[30] The respective monolith was stirred in 500 mL 0.01 N NaOH solution. 30 mL of the resulting solution was then titrated with 0.01 N HCl solution, using phenolphthalein as indicator. With the known starting concertation of NaOH and the amount of required HCl the sulfonation degree was calculated.

Batch hydrolysis of sucrose

In a glass reactor with a 3D printed inset to fix the catalytic monoliths in the solution (see supporting information Figure S6) the respective catalyst was tested at a temperature of 79 °C and a stirring rate of 500 rpm. The initial sucrose concentration was 50 g L^{-1} with a total volume of 150 mL.

Continuous hydrolysis of sucrose

For this setup a tubular reactor with a diameter of 3 cm and a length of 17 cm was used in the setup as displayed in Figure S7 (see supporting information). The feed solution was pumped with flow rates of 0.5–8.0 mL min^{-1} and an initial sucrose concentration of 50 g L^{-1}. The direction of the flow was from bottom to top of the reactor to ensure the full immersion of the catalyst surface. The reactor was heated to 80 °C.

HPLC characterization

A high-performance liquid chromatography (HPLC) unit type *Nexera XR* (Shimadzu Corporation) with an *Aminex HPX-87 C Carbohydrate* column (Bio Rad) was used for quantitative analysis of the reaction mixture. The column temperature was set to 80 °C and *MilliQ-pure water* was used as eluent with a flow rate of 0.6 mL min^{-1}. For analysis, an online refractive index detector (RID) was used. Calibration was done with different concentration series of the sucrose, fructose and glucose solutions, respectively.

Acknowledgements

We gratefully acknowledge financial support by the German Federal Ministry of Education and Research (BMBF Grant No. 031B0678B). Open Access funding enabled and organized by Projekt DEAL.

Conflict of Interest

The authors declare no conflict of interest.

Data Availability Statement

The data that support the findings of this study are available from the corresponding author upon reasonable request.

© 2022 The Authors. ChemCatChem published by Wiley-VCH GmbH

18673899, 2022, 8, Downloaded from https://chemistry-europe.onlinelibrary.wiley.com/doi/10.1002/cctc.202101947 by Technische Universitat Darmstadt, Wiley Online Library on [18/09/2023]. See the Terms and Conditions (https://onlinelibrary.wiley.com/terms-and-conditions) on Wiley Online Library for rules of use; OA articles are governed by the applicable Creative Commons License

Keywords: 3D printing · additive manufacturing · catalyst monolith · acid catalysis · hydrolysis

[1] C. Fee, S. Nawada, S. Dimartino, *J. Chromatogr. A* **2014**, *1333*, 18–24.
[2] A. Daneyko, A. Höltzel, S. Khirevich, U. Tallarek, *Anal. Chem.* **2011**, *83*, 3903–3910.
[3] S. Khirevich, A. Daneyko, A. Höltzel, A. Seidel-Morgenstern, U. Tallarek, *J. Chromatogr. A* **2010**, *1217*, 4713–4722.
[4] A. Cybulski, J. A. Moulijn, *Structured catalysts and reactors*, CRC press, **2005**.
[5] A. Daneyko, S. Khirevich, A. Höltzel, A. Seidel-Morgenstern, U. Tallarek, *J. Chromatogr. A* **2011**, *1218*, 8231–8248.
[6] M. Klumpp, A. Inayat, J. Schwerdtfeger, C. Körner, R. F. Singer, H. Freund, W. Schwieger, *Chem. Eng. J.* **2014**, *242*, 364–378.
[7] Y. Li, S. Chen, X. Cai, J. Hong, X. Wu, Y. Xu, J. Zou, B. H. Chen, *J. Mater. Chem. A* **2018**, *6*, 5695–5702.
[8] S. Didierjean, H. P. A. Souto, R. Delannay, C. Moyne, *Chem. Eng. Sci.* **1997**, *52*, 1861–1874.
[9] H. Eghbali, V. Verdoold, L. Vankeerberghen, H. Gardeniers, G. Desmet, *Anal. Chem.* **2008**, *81*, 705–715.
[10] N. V. Lavrik, L. C. Taylor, M. J. Sepaniak, *Lab Chip* **2010**, *10*, 1086–1094.
[11] J. L. Williams, *Catal. Today* **2001**, *69*, 3–9.
[12] M. Hettel, C. Antinori, O. Deutschmann, *Emiss. Control Sci. Technol.* **2016**, *2*, 188–203.
[13] K. Iida, S. Nojima, Y. Obayashi, A. Morii, O. Naito, **2000**, US6156698 A.
[14] J. N. Stuecker, J. E. Miller, R. E. Ferrizz, J. E. Mudd, J. Cesarano, *Ind. Eng. Chem.* **2004**, *43*, 51–55.
[15] C. Y. Chaparro-Garnica, P. Jordá-Faus, E. Bailón-García, R. Ocampo-Pérez, C. G. Aguilar-Madera, A. Davó-Quiñonero, D. Lozano-Castelló, A. Bueno-López, *ACS Appl. Mater. Interfaces* **2020**, *12*, 54573–54584.
[16] J. A. Moulijn, M. T. Kreutzer, T. A. Nijhuis, F. Kapteijn, *Advances in Catalysis, Vol. 54*, Elsevier, **2011**, pp. 249–327.
[17] T. J. Schildhauer, F. Kapteijn, J. A. Moulijn, *Ind. Eng. Chem. Res.* **2005**, *44*, 9556–9560.
[18] S. Hock, M. Rose, *Chem. Ing. Tech.* **2020**, *92*, 525–531.
[19] S. Hajimirzaee, A. M. Doyle, *Fuel* **2020**, 274, 117848.
[20] S. Lawson, A. Farsad, B. Adebayo, K. Newport, K. Schueddig, E. Lowrey, F. Polo-Garzon, F. Rezaei, A. A. Rownaghi, *Adv. Sustainable Syst.* **2021**, 5, 2000257.
[21] E. Bogdan, P. Michorczyk, *Materials* **2020**, 13, 4534.
[22] P. J. Kitson, M. D. Symes, V. Dragone, L. Cronin, *Chem. Sci.* **2013**, *4*, 3099–3103.
[23] M. Guvendiren, J. Molde, R. M. Soares, J. Kohn, *ACS Biomater. Sci. Eng.* **2016**, *2*, 1679–1693.
[24] A. Ambrosi, M. Pumera, *Chem. Soc. Rev.* **2016**, *45*, 2740–2755.
[25] B. Utela, D. Storti, R. Anderson, M. Ganter, *J. Manuf. Process.* **2008**, *10*, 96–104.
[26] C. Minas, D. Carnelli, E. Tervoort, A. R. Studart, *Adv. Mater.* **2016**, *28*, 9993–9999.
[27] X. Zhou, C.-j. Liu, *Adv. Funct. Mater.* **2017**, *27*, 1701134.
[28] C. Parra-Cabrera, C. Achille, S. Kuhn, R. Ameloot, *Chem. Soc. Rev.* **2018**, *47*, 209–230.
[29] S. Lawson, X. Li, H. Thakkar, A. A. Rownaghi, F. Rezaei, *Chem. Rev.* **2021**, *121*, 6246–6291.
[30] P. Dudek, *Arch. Metall. Mater.* **2013**, *58*, 1415–1418.
[31] J. A. Lewis, *Adv. Funct. Mater.* **2006**, *16*, 2193–2204.
[32] T. Tabassum, M. Iloska, D. Scuereb, N. Taira, C. Jin, V. Zaitsev, F. Afshar, T. Kim, *J. Chem. Educ.* **2018**, *95*, 783–790.
[33] C. R. Tubío, J. Azuaje, L. Escalante, A. Coelho, F. Guitián, E. Sotelo, A. Gil, *J. Catal.* **2016**, *334*, 110–115.
[34] M. Zhang, L. Li, Q. Lin, M. Tang, Y. Wu, C. Ke, *J. Am. Chem. Soc.* **2019**, *141*, 5154–5158.
[35] M. R. Skorski, J. M. Esenther, Z. Ahmed, A. E. Miller, M. R. Hartings, *Sci. Technol. Adv. Mater.* **2016**, *17*, 89–97.
[36] X. Sun, Y. Yan, L. Zhang, G. Ma, Y. Liu, Y. Yu, Q. An, S. Tao, *Adv. Mater. Interfaces* **2018**, *5*, 1701626.
[37] C. Zhu, Z. Qi, V. A. Beck, M. Luneau, J. Lattimer, W. Chen, M. A. Worsley, J. Ye, E. B. Duoss, C. M. Spadaccini, C. M. Friend, J. Biener, *Sci. Adv.* **2018**, *4*, eaas9459.
[38] A. Ahlawat, R. K. Sahdev, R. K. Gupta, D. Chhabra, *Nano-Electron. Phys.* **2021**, 13.
[39] L. P. Bressan, T. M. Lima, G. D. da Silveira, J. A. F. da Silva, *SN Appl. Sci.* **2020**, 2, 984.
[40] V. Tambrallimath, R. Keshavamurthy, D. Saravanabavan, P. G. Koppad, G. P. Kumar, *Compos. Commun.* **2019**, 15, 129–134.
[41] Y.-l. Lei, Y.-j. Luo, F. Chen, L.-h. Mei, *Polymer* **2014**, *6*, 1914–1928.
[42] A. Al-Sabagh, Y. Moustafa, A. Hamdy, H. Killa, R. Ghanem, R. Morsi, *Egypt. J. Pet.* **2018**, *27*, 403–413.
[43] K. Lienkamp, I. Schnell, F. Groehn, G. Wegner, *Macromol. Chem. Phys.* **2006**, *207*, 2066–2073.
[44] R. Brückner, *Reaktionsmechanismen: organische Reaktionen, Stereochemie, moderne Synthesemethoden*, Springer-Verlag, **2014**.
[45] J. E. Coughlin, A. Reisch, M. Z. Markarian, J. B. Schlenoff, *J. Polym. Sci. Part A* **2013**, *51*, 2416–2424.
[46] B. H. Bakker, H. Cerfontain, *Tetrahedron Lett.* **1989**, *30*, 5451–5454.
[47] L. Sandbrink, T. Lazaridis, M. Rose, R. Palkovits, *Microporous Mesoporous Mater.* **2018**, *267*, 198–202.
[48] P. M. Leininger, M. Kilpatrick, *J. Am. Chem. Soc.* **1938**, *60*, 2891–2899.
[49] E. Anklam, *Anal. Bioanal. Chem.* **2005**, *382*, 10–11.
[50] H. Iloukhani, S. Azizian, N. Samadani, *Phys. Chem. Liq.* **2002**, *40*, 159–165.
[51] K. Zajšek, A. Goršek, *React. Kinet. Mech. Catal.* **2010**, *100*, 265–276.
[52] P. W. Atkins, J. De Paula, J. Keeler, *Atkins' physical chemistry*, Oxford university press, **2018**.
[53] C. Buttersack, D. Laketic, *Studies in Surface Science and Catalysis, Vol. 98*, Elsevier, **1995**, pp. 190–191.
[54] H. Iloukhani, S. Azizian, N. Samadani, *React. Kinet. Catal. Lett.* **2001**, *72*, 239–244.
[55] J. Pérez-Maqueda, I. Arenas-Ligioiz, Ó. López, J. G. Fernández-Bolaños, *Chem. Eng. Sci.* **2014**, *109*, 244–250.
[56] A. Takagaki, M. Nishimura, S. Nishimura, K. Ebitani, *Chem. Lett.* **2011**, *40*, 1195–1197.
[57] W. Yu, K. Hidajat, A. K. Ray, *Appl. Catal. A* **2004**, 260, 191–205.
[58] Amberlyst 15; MSDS No. 115635 [Online]; *Merck KGaA* Darmstadt, Ger, **2014**. https://www.merckmillipore.com/DE/de/product/msds/MDACHEM-115635?Origin=PDP (accessed 4/15/20).

Manuscript received: December 22, 2021
Revised manuscript received: January 31, 2022
Accepted manuscript online: January 31, 2022
Version of record online: March 1, 2022

© 2022 The Authors. ChemCatChem published by Wiley-VCH GmbH

18673899, 2022, 8, Downloaded from https://chemistry-europe.onlinelibrary.wiley.com/doi/10.1002/cctc.202101947 by Technische Universitat Darmstadt, Wiley Online Library on [18/09/2023]. See the Terms and Conditions (https://onlinelibrary.wiley.com/terms-and-conditions) on Wiley Online Library for rules of use; OA articles are governed by the applicable Creative Commons License